Dynamics of gaseous material ejection following laser breakdown on the surface of CaF2

S. G. Demos, R. A. Negres, A. M. Rubenchik

July 22, 2013

Applied Physics

Disclaimer

Dynamics of gaseous material ejection following laser breakdown on the surface of CaF$_2$

Stavros G. Demos*, Raluca A. Negres, Alexander M. Rubenchik

Lawrence Livermore National Laboratory, 7000 East Ave, Livermore, CA, USA 94550

* demos1@llnl.gov

ABSTRACT

The temporal evolution of the gaseous material ejection during laser ablation in Calcium fluoride at ambient atmospheric conditions is investigated using time-resolved microscopy. The results demonstrate the important role of gaseous material expansion in the formation of the shockwave and suggest that the production of gaseous materials is prolonged, extending well after the termination of the laser pulse. In addition, we capture the backward motion of the gaseous material cloud after its initial expansion settling within a narrow zone near the surface where it remains for tens of microseconds.

Subject Terms: Time-resolved microscopy, laser radiation effects, laser-induced breakdown, ablation plume kinetics, insulators.

Laser ablation is currently a well-established method for materials' processing, manufacturing and characterization and it is widely used as a research tool. Laser ablation is also part of parasitic processes such as in laser-induced damage on the surface of optical materials which is typically initiated by light absorbing defects. One of the important aspects of laser ablation is the production of a backward-deposited layer of the ablated material around the laser irradiated region. This behavior has been attributed to confinement of the plasma formed near the surface [1-4]. A number of reports have discussed the properties of the debris following long (ns) or short (fs) pulse laser ablation in various materials including dielectrics, metals, and semiconductors [5–8]. Simple analytical models have been suggested to describe the interaction of a laser-generated plasma plume with a background gas as well as the backward flow of laser ablated material leading to inverse pulsed laser deposition [9-11]. Time resolved imaging of the plasma emission [12] has captured the backward flux of ionized material to which the material deposition process was attributed. In addition, it was hypothesized that the drag forces generated on smaller and slower particles can affect their trajectory and subsequent deposition near the ablation site. [13-14]. In the context of laser damage on the surface of fused silica optics, some of the ejected particles with diameter on the order of 10 μm were shown to abruptly change direction, with backward motion towards the surface; it was also estimated that an airflow wave with speed on the order of 100 m/s was required to cause this effect [15].

The particles ejected during the ablation process are slower than the atomic evaporants [16]. At ambient conditions, the generation and expansion of the shockwave is accompanied by the ejection of particles. Images captured at early pump-probe delays following damage initiation (or laser ablation) of various materials demonstrate that the axial expansion of the shockwave is considerably faster than its lateral expansion [17,18].. A recent study for the case of fused silica

demonstrated time-resolved images of surface swelling prior to the ejection of micro-scale particles, causing a delay in the ejection process by about 30 ns [17]. It was also shown that the ejection process continues for much longer duration than that of the laser pulse [18]. These observations highlight the complex processes involved in the material response to the laser energy deposition that are still not well understood.

This work captures the complex dynamics of the gaseous material ejection during laser induced breakdown on the surface of Calcium fluoride (CaF_2). A gaseous material cloud is clearly visible with time resolved shadowgraphic microscopy enabling the study of the dynamics of the gaseous material ejection, especially at early times, and how it affects the generation and propagation of the shockwave.. This behavior observed in CaF_2 is characteristically different form many other transparent materials we have tested using the same experimental configuration which exhibited a behavior similar to that reported in fused silica [18]. The clarity of the images captured along with the fact that the gaseous material ejection is not hindered by the ejection of micro-scale particles makes this material ideal for studying the plume expansion process originating from breakdown/ablation from very small areas. To the best of our knowledge, this work provides the most detailed experimental results to date of this process. A detailed quantification of the kinetics of the gaseous material expansion and subsequent contraction is provided.

Time resolved images of the ejected material were captured by shadowgraphic imaging using a time-resolved microscope system described in detail elsewhere [19]. In brief, breakdown was induced on the exit-surface of a 2.5-cm round, 1-cm thick CaF_2 optical window with polished sides by focusing a laser pulse (henceforth referred to as *pump* pulse) about 1 cm behind the optic's exit-surface as shown in Fig. 1(a). The pump laser was operating at 1064 nm with pulse duration of 10-ns full-width at half maximum (FWHM) intensity and an average fluence of the

converging beam at the exit surface location on the order of 1 KJ/cm^2 by means of a 10 cm focal length lens. The beam was propagating through the sample to initiate breakdown on the exit surface in order to avoid interaction of the ejected material with the laser pulse. The side of the sample was illuminated with two spatially overlapped, orthogonally polarized 532 nm, 4.5 ns FWHM *probe* laser pulses. Each probe pulse was delayed with respect to the peak of the pump pulse via adjustable external triggers, allowing side-view illumination of the sample at two time points during a single laser energy deposition event. A composite 5X zoom and 5X objective lens system was used to collect the dual-probe signal traversing the ejected material volume; this signal was subsequently passed through a 532-nm narrowband filter and separated into its constituent polarization components using a polarizing beam-splitter. Thus each component arising from a different probe captures the dynamics of the ejected material at a different delay. Images from each probe beam were recorded by separate charge-coupled device (CCD) cameras. Static optical resolution was better than 2 μm with a depth of focus of ~40 μm.

Representative experimental results of the microscopic shadowgraphic images are shown in Figs. 1 and 2. CaF$_2$ exhibits a very visible, expanding at high-speed "gaseous" ejected material originating at the surface location of breakdown. On the other hand, the ejection of micro scale particles is very limited and the observed particles have low initial ejection speeds. Such particles can be seen for example in Fig. 2(a) at 800 ns delay, with the particles located within about 400 μm from the surface, suggesting a speed of less than about 500 m/s compared to speeds on the order of up to 2 km/s or larger observed in fused silica and other materials. As a result, the ejected particles in CaF$_2$ do not interfere in any way with the initial expansion of the gaseous material.

During the experiments, one probe delay was always fixed at 800 ns as a reference for the

amount of gaseous material and its expansion from the surface. These characteristics of the gaseous ejection allowed selection of similar laser deposition events, as these events can vary between different surface locations and are sensitive to fluctuations in the pump laser fluence. Thus the analysis is based on events which exhibited an expansion at 800 ns delay similar to that observed in Fig. 2(a) and are representative of laser fluences near the damage threshold of the material. We hypothesize that this gaseous material contains a sufficiently large number of nanoparticles which scatter the probe light and create the observed "shadow". The probe light obscuration was as high as about 70% but the images retained their polarization state (no significant cross-talk in our orthogonal polarization detection scheme) suggesting that the image is formed by ballistic (probe beam) light propagating through the gaseous material. This in turn means that the size of the particles is much smaller than the probe laser wavelength (532 nm) since large-angle scattering dominates [20]. Such small particles are frozen into the flow and provide the flow visualization.

The experimental results in Fig. 1 capture the initial rapid expansion phase and the development of the "mushroom cloud" at about 150 ns delay. The surrounding air decelerates the expansion while the interface between the ejected gaseous material and the ambient gas is unstable [21], similar to the Rayleigh-Taylor instability visible in Fig. 1. The observed instabilities appear to be saturated on the low level of perturbations and do not produce a noticeable mixing, probably due to the compressibility of the air that causes attenuation of the instability effects.

The "mushroom cloud" remains connected to the surface of the material where breakdown took place with a narrow conduit of gaseous material for more than 300 ns as shown in Fig. 1(e). At the same time, the size (volume) of this "mushroom cloud" increases without a corresponding increase in the amount of light penetrating through it. These observations suggest that the cloud

is constantly supplied with additional gaseous material for an extended period of time, well after the termination of the laser pulse. The image captured at 500 ns (Fig 1f) shows the dissipation of the gaseous conduit.

The location of the ensuing shockwave propagating in the air is also visible in the images of Fig. 1, as indicated by the arrows. The simultaneous observation of the boundaries of the gaseous material and that of the shockwave as a function of delay enables better understanding of the processes leading to the formation of the shockwave. Specifically, from the early delay times, the expansion of the gaseous material is directional, mostly orthogonal to the surface of the sample. As a result, a separation between the boundaries of the gaseous material and that of the shockwave is perceptible near the surface of the sample (lateral direction), even at 30 ns delay (Fig. 1a). On the other hand, a separation between the boundaries in the direction orthogonal to the surface of the sample (axial direction) is observed at about 100 ns delay and thereafter continuously increases with delay time. During this period of time, the shockwave developed an elongated propagation, with the radius of the shockwave near the surface of the sample approximately 0.55 its maximum distance from the surface. This indicates that the directional expansion of the gaseous material affects the formation and propagation of the shockwave.

Due to their small size, the motion of the particles comprising the observed "cloud" is controlled by the motion of the surrounding vapor material (air and vaporized ablated material). Figure 2 demonstrates that after the initial expansion of the ejected gaseous material, the size of the gaseous cloud stabilizes at about 1.7 mm from the surface. Subsequently, there is a backward motion towards the surface where an approximately 500 μm layer of gaseous material is forming by about 10 μs delay. The experiments showed that this layer starts "dissipating" after 20 μs delay; the probe beam obscuration is reduced to about half at 25 μs delay and becomes nearly

invisible by 30 μs delay. This is attributed in part to the diffusion of the gaseous material along the surface and is similar to the observations reported by imaging the plasma emission of the ablation plume [12].

The dynamic profile of the gaseous material cloud is captured in Figure 3 where the distance from the surface and the speed of expansion (along the axial direction) are plotted as a function of the delay time. The initial speed of expansion is on the order of 10 km/s and decreases to about 1 km/s after about 300 ns. The speed becomes negative (backward motion towards the surface) at about 3 μs delay and returns to zero after about 10 μs.

After the pulse termination, the high pressure cloud of ejected material is expanding in the surrounding gas having much lower pressure. The boundary velocity u is given by expression

$u = \frac{2}{\gamma-1}\sqrt{\frac{\gamma P}{\rho}}$ [22] where ρ is the material density (ρ=3.2 g/cm^3 for CaF$_2$), P is the pressure and

γ is the adiabatic constant (γ=7/5 for air). Given that the initial observed speed is about 10 km/s (see Fig. 3), the initial pressure is estimated at about 6.3 GPa.

During the expansion phase, the interior pressure declines as $1/R^3$ until it reaches the outside atmospheric pressure, at which point the expansion terminates. This takes place at

$R \sim \left(\frac{E}{p_0}\right)^{1/3}$ [22] where E is the energy released during micro-explosion and p_0 is the atmospheric

pressure. In our experiments, R is about 1700 μm. This implies that the energy released is about 1 mJ. This estimate represents an upper limit as the theoretical formulation assumes a spherical expansion while the experiment suggests a more directional expansion (axially). SEM and optical images of the ensuing damage sites suggest that the affected area was on the order of 2x10^4 μm^2 but a visible crater (due to material ejection) covers an area on the order of 4x10^3 μm^2. From laser beam profiling diagnostics, we estimate that this central ablated region was

exposed to about 1.75 mJ of laser power. Assuming that all the energy released originated from this central region, the results suggest that up to about 50% of the laser energy was spent in the expansion of the gaseous material.

The results presented in this work provide new information on the dynamics of plume formation during laser ablation. It is also directly related to the processes involved during laser-induced damage on the surface of optical materials and helps better understand our previous observations. Specifically for the case of fused silica, the observed non-symmetric expansion of the shockwave at early delays [17, 18] is attributed to the piston-like compression of the surrounding air by the directionally expanding gaseous plume behind it (not visible in this case). Also, this work confirms that the gaseous material does not expand beyond about 2 mm from the surface at ambient conditions. Therefore the emission observed in fused silica at distances on the order of 4 mm from the ablation site [15] is indeed due to the emission by hot ejected particles, leading to an estimated temperature at the center of these particles on the order of 0.5 eV. The gaseous material back-flow with a maximum speed on the order of 100 m/s can explain the change in the trajectory of smaller slower particles (on the order of 1-20 μm in diameter) that are subsequently directed backward towards the surface [13-15]. These results also indicate the extent of zone of debris redeposition.

References

[1] A. Miotello, R. Kelly, B. Braren, and C. E. Otis, Appl. Phys. Lett. **61**, 2784 , 1992.

[2] I. A. Movtchan, R. W. Dreyfus, W. Marine, M. Sentis, M. Autric, G. Le Lay, and N. Merk, Thin Solid Films **255**, 286, 1995.

[3] L. Patrone, D. Nelson, V. I. Safarov, M. Sentis, W. Marine, and S. Giorgio, J. Appl. Phys. **87**, 3829, 2000.

[4] A. Pereira, A. Cros, P. Delaporte, S. Georgiou, A. Manousaki, W. Marine, and M. Sentis, Appl. Phys. A **79**, 1433, 2004.

[5] J. Heitz, J.T. Dickinson, Appl. Phys. A **68**, 515, 1999.

[6] S. Eliezer, N. Eliaz, E. Grossman, D. Fisher, I. Gouzman, Z. Henis, S. Pecker, Y. Horovitz, M. Fraenkel, S. Maman, and Y. Lereah, Phys. Rev. B **69**, 144119 , 2004.

[7] S. Singh, M. Argument, Y.Y. Tsui, R. Fedosejevs, J. Appl. Phys. **98**, 113520, 2005.

[8] S. Ku☐per, J. Brannon, Appl. Phys. Lett. **60**, 1633, 1992.

[9] A A Morozov, Z. Geretovszky and T. Szörényi, J. Phys. D: Appl. Phys. **41**, 015303, 2008.

[10] Tatiana E. Itina, Jorg Hermann, Philippe Delaporte, and Marc Sentis, Phys. Rev. E **66**, 066406 , 2002.

[11] Sobieslaw Gacek and Xinwei Wang, J. Appl. Phys.**104**, 126101, 2008.

[12] A. Pereira, P. Delaporte, M. Sentis, W. Marine, A. L. Thomann and C. Boulmer-Leborgne, J. Appl. Phys. **98**, 064902,_2005.

[13] G. Koren and U. P. Oppenheim, Appl. Phys. B **42**, 41, 1987.

[14] A. Miotello, R. Kelly, B. Braren, and C. E. Otis, Appl. Phys. Lett. **61**, 2784, 1992.

[15] R. N. Raman, S. Elhadj, R. A. Negres, M. J. Matthews, M. D. Feit, and S. G. Demos, Opt.

Express, **20**, 27720, 2012.

[16] H. Dupendant, J.P. Gavigan , D. Givord, A. Lienard, J.P. Rebouillat and Y. Souche, Appl. Surf. Sci., **43**, 369, 1989.

[17] S. G. Demos, R. A. Negres, R. N. Raman, A. M. Rubenchik, M. D. Feit, Laser and Phot. Rev., **7**, 444, 2013.

[18] S. G. Demos, R. N. Raman and, R. A. Negres , Opt. Express, **21**, 4875, 2013.

[19] R. N. Raman, R. A. Negres, and S. G. Demos, Opt. Eng. **50**, 013602, 2011.

[20] H. Van de Hulst, " Light scattering by small particles", Dover Publications. (New York, 1981)

[21] S. I.Anisimov, V.A.Khokhlov, "Instabilities in laser-matter interaction", CRC Press, 2000

[22] Ya. B. Zeldovich, Yu. P. Raizer, "Physics of Shock Waves and High Temperature Hydrodynamic Phenomena", Academic Press, New York,1967

Figure Captions

Figure 1. (a)-(f) Shadowgraphic images capturing the expansion of the ejected gaseous material in CaF_2 at a) 30 ns, b) 70 ns, c) 100 ns, d) 150 ns, e) 300 ns and, f) 500 ns delays. Air is on the left side of each image and the gray-black interface represents the surface of the material; the laser beam propagates from right to left. Arrows indicate the position of the shockwave in the axial and lateral directions. The spatial calibration bar applies to all images.

Figure 2. (a)-(f) Shadowgraphic images capturing the position of the gaseous material at a) 800 ns, b) 3.5 µs, c) 6 µs, d) 11 µs, e) 16 µs and, f) 21 µs delays. The spatial calibration bar applies to all images.

Figure 3. The distance of the gaseous material cloud from the surface (right axis) and its expansion (and retraction) speed (left axis) as a function of the delay time
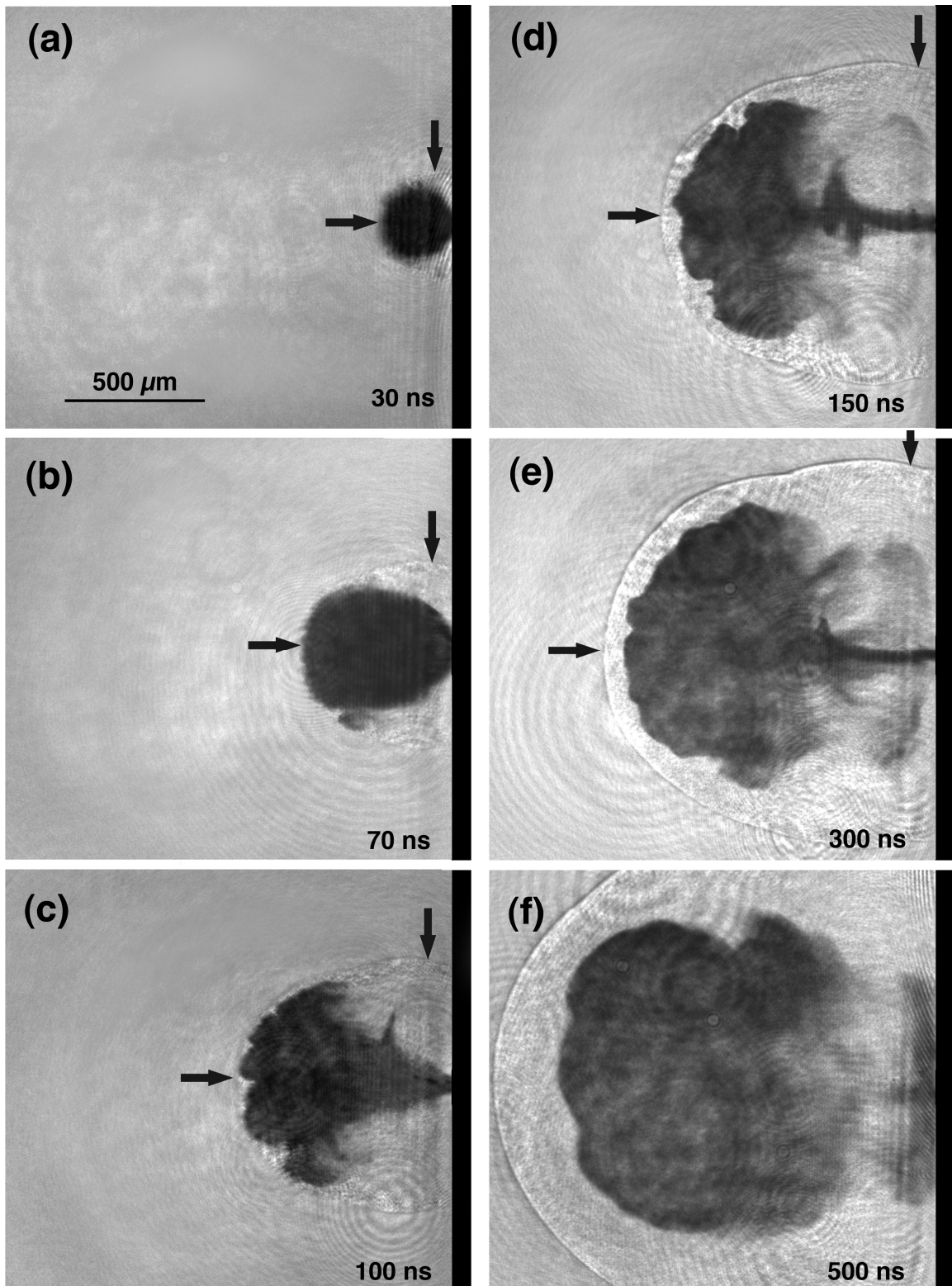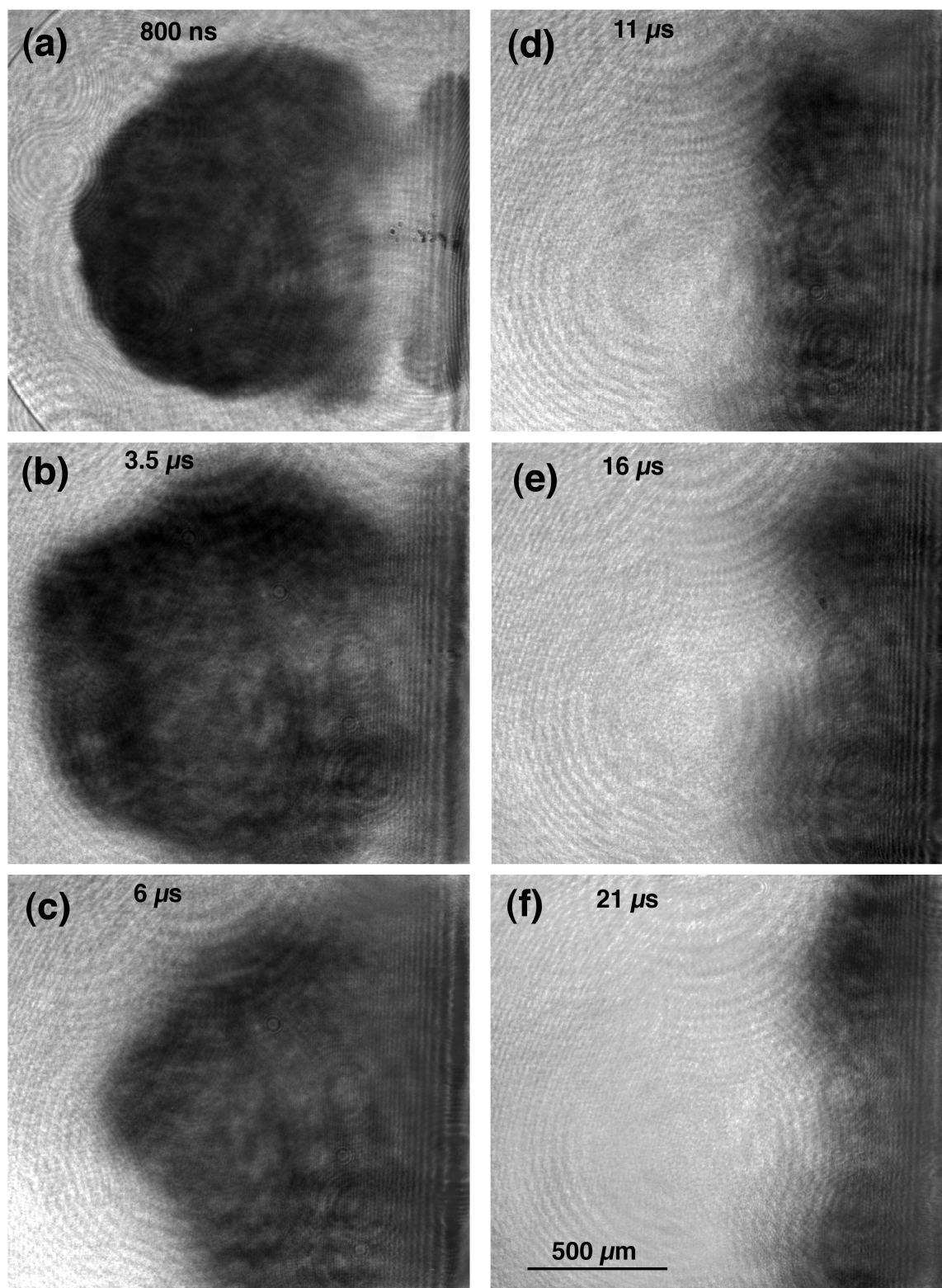
500 μm

(a) 30 ns
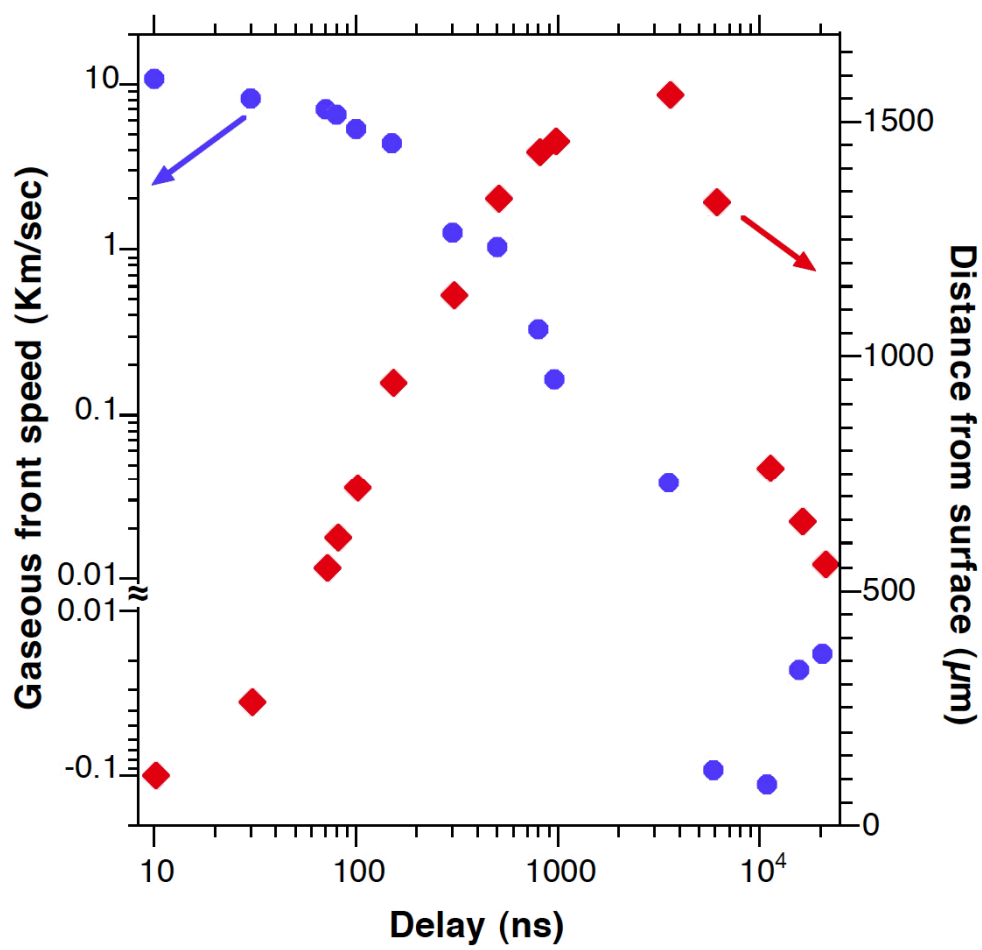(b) 70 ns
(c) 100 ns
(d) 150 ns
(e) 300 ns
(f) 500 ns

FIGURE 1

12

(a) 800 ns

(b) 3.5 μs

(c) 6 μs

(d) 11 μs

(e) 16 μs

(f) 21 μs

500 μm

FIGURE 2

13

FIGURE 3